Comparison of abnormal isoform of prion protein in prion-infected cell lines and primary cultured neurons by PrP^{Sc}-specific immunostaining

Running title: PrP^{Sc} in immortalized cell lines and primary neurons

Misaki Tanaka[1], Ai Fujiwara[1], Akio Suzuki[1], Takeshi Yamasaki[1], Rie Hasebe[1], Kentaro Masujin[2, 3] and Motohiro Horiuchi[1]

[1]Laboratory of Veterinary Hygiene, Graduate School of Veterinary Medicine, Hokkaido University, Kita 18, Nishi 9, Kita-ku, Sapporo 060-0818, Japan

[2]National Agriculture Food Research Organization (NARO), 3-1-5 Kannondai, Tsukuba, Ibaraki, 305-0856, Japan and [3]Laboratory of Persistent Viral Diseases, Rocky Mountain Laboratories, National Institute for Allergy and Infectious Diseases, National Institutes of Health, Hamilton, MT, USA

Correspondence to: Motohiro Horiuchi, DVM, Ph.D.
Laboratory of Veterinary Hygiene,
Graduate School of Veterinary Medicine,
Hokkaido University,
Kita 18, Nishi 9, Kita-ku,
Sapporo 060-0818, Japan
Phone/Fax: +81-11-706-5293

Subject category: TSE agents

Keywords: prions, Immunofluorescence assay, primary neurons, guanidine isothiocyanate, monoclonal antibody

Word count: abstract (238), main text (4,708)

Abbreviations:

Ara-C ,cytosine arabinoside; CNs, primary cerebral neurons; DAPI 4',6-Diamidino-2-phenylindole; div, days in vitro; dpi, days post infection; GdnSCN, guanidine isothiocyanate; GFAP, glial fibrillary acidic protein; IFA, immunofluorescence assay; MAP2, microtubule-associated protein 2; N2a, Neuro2a; pAbs; polyclonal antibodies; PK, proteinase K; PrP^{C}; cellular isoform of prion protein; PrP^{Sc}; abnormal isoform of prion protein; PrP-res, proteinase K-resistant PrP^{Sc}; PTA, phosphotungstic acid; RT, room temperature; ScGT1-7-22L, GT1-7 persistently infected with the 22L prion strain; ScN2a-3-22L, N2a-3 persistently infected with the 22L prion strain; ScN2a-3-Ch, N2a-3 persistently infected with the Chandler prion strain

Abstract

We established abnormal isoform of prion protein (PrP^{Sc})-specific double immunostaining using mAb 132 that recognizes aa 119–127 of the PrP molecule and novel PrP^{Sc}-specific mAb 8D5 that recognizes the N-terminal region of the PrP molecule. Using the PrP^{Sc}-specific double immunostaining, we analyzed PrP^{Sc} in immortalized neuronal cell lines and primary cerebral neuronal cultures infected with prions. The PrP^{Sc}-specific double immunostaining showed the existence of PrP^{Sc} positive for both mAbs 132 and 8D5 as well as those positive only for either mAb 132 or mAb 8D5. This indicated that double immunostaining detects a greater number of PrP^{Sc} species than single immunostaining. Double immiunostaining revealed cell type-dependent differences in PrP^{Sc} staining patterns. In the 22L prion strain-infected Neuro2a (N2a)-3 cells, a subclone of N2a neuroblastoma cell line, or GT1-7, a subclone of the GT1 hypothalamic neuronal cell line, granular PrP^{Sc} stains were observed at the perinuclear regions and cytoplasm, whereas unique string-like PrP^{Sc} stains were predominantly observed on the surface of the 22L strain-infected primary cerebral neurons. Only 14% of PrP^{Sc} in the 22L strain-infected N2a-3 cells were positive for mAb 8D5, indicating that most of the PrP^{Sc} in N2a-3 lack the N-terminal portion. In contrast, nearly half PrP^{Sc} detected in the 22L strain-infected primary cerebral neurons were positive for mAb 8D5, suggesting the abundance of full-length PrP^{Sc} that possesses the N-terminal portion of PrP. These results pose a problem in interpreting the mechanism of prion propagation in different cell types.

Introduction

Transmissible spongiform encephalopathies, also known as prion diseases, are fatal neurodegenerative disorders in humans and animals, which are caused by the infectious agent called prions. The pathological hallmarks of prion diseases include microglial activation, astrogliosis, and accumulation of abnormal isoform of prion protein (PrP^{Sc}) in the central nervous system. PrP^{Sc} is generated from a host-encoded cellular isoform of prion protein (PrP^{C}) by posttranslational modifications such as conformational transformation (Prusiner, 1998). The generation of PrP^{Sc} is believed to be strongly associated with prion propagation and neurodegeneration in prion diseases (Mallucci *et al.*, 2003). Therefore, the clarification of the cellular mechanism of PrP^{Sc} formation would be useful.

Cell biological studies using immortalized neuronal cell lines such as Neuro2a (N2a) neuroblastoma and GT1 hypothalamic neuronal cells have greatly contributed to the elucidation of the cellular mechanism underlying prion propagation. Earlier studies suggested that PrP^{Sc} is generated from mature PrP^{C} expressed on the cell surface and that the PrP^{Sc} generation occurs at cellular compartments on the endocytotic pathway including the cholesterol-rich membrane microdomain called lipid rafts (Borchelt *et al.*, 1992; Caughey & Raymond, 1991; Naslavsky *et al.*, 1997; Vey *et al.*, 1996). Further cell biological studies within a decade indicated the involvement of endocytic recycling compartments and endocytic recycling pathway in PrP^{Sc} formation (Beranger *et al.*, 2002; Marijanovic *et al.*, 2009; Pimpinelli *et al.*, 2005; Veith *et al.*, 2009; Yamasaki *et al.*, 2012). We recently reported that after the inoculation of prions, newly generated PrP^{Sc} appeared on the cell surface, early endosomes, and late endosomes of N2a cells (Yamasaki *et al.*, 2014a). These cell biological studies suggest the intracellular vesicular compartments to be the major sites for PrP^{Sc}

87 formation, whereas it was reported that PrP^{Sc} formation occurs on the cell surface within a
88 minute (Goold *et al.*, 2011). On the other hand, ultrastructural studies using the brains of
89 prion-infected mice showed that PrP^{Sc} was frequently detected on the plasma membranes of
90 neuropils but occasionally in the intracellular vesicles (Godsave *et al.*, 2008; Godsave *et al.*,
91 2013; Jeffrey *et al.*, 1994; Jeffrey *et al.*, 1992). Further immuno-electron microscopic studies
92 using anti-PrP recognizing the N-terminal region of PrP suggested that neuronal plasma
93 membranes such as membrane invaginations and sites of cell-to-cell contact are primary sites
94 for PrP^{Sc} formation (Godsave *et al.*, 2013). To resolve the partly contradictory results
95 regarding the site of PrP^{Sc} formation between cell culture and ultrastructural studies, primary
96 cultured neurons are considered to be a good *ex vivo* model. There are only a few reports on
97 prion propagation in primary cultured neurons derived from the cerebellum, striatum, and
98 cerebral cortex of mouse brains (Cronier *et al.*, 2004; Dron *et al.*, 2010; Hannaoui *et al.*,
99 2013). However, little information is available on the localization of PrP^{Sc} in primary neurons
100 infected with prions.

101 Taraboulos et al. reported that treatment of fixed cells with guanidinium salts prior to
102 incubation with anti-PrP antibodies significantly increases the PrP^{Sc} signals in
103 immunocytochemical staining (Taraboulos *et al.*, 1990). This method has been being used for
104 PrP^{Sc}-specific detection by immunofluorescence assay (IFA). However, careful adjustment of
105 the threshold level by manipulation of the detector gain or the exposure time is required for
106 the discrimination of PrP^{Sc} signals from PrP^{C}. One concern to arise is that such manipulations
107 may limit the detailed analysis of PrP^{Sc}. We recently reported that mAb 132 recognizing the
108 epitope comprising mouse PrP aa 119–127 distinguishes PrP^{Sc} from PrP^{C} in prion-infected
109 cells and tissues with a minimum manipulation of threshold setting (Sakai *et al.*, 2013;

Yamasaki *et al.*, 2012). Although the pretreatment with guanidinium salts is still prerequisite, the advantage in threshold setting made it possible to disclose the detailed intracellular localization of PrP^{Sc} in cells persistently infected with prions (Yamasaki *et al.*, 2014a; Yamasaki *et al.*, 2014b; Yamasaki *et al.*, 2012). The use of mAb 132 improved the specificity of PrP^{Sc} detection; however, PrP^{Sc} comprises a heterologous PrP^{Sc} population in the size and rigidity of aggregates. Therefore, whether mAb 132 can detect all of PrP^{Sc} species in cells remains obscure.

Recently, Masujin and his colleagues reported a new PrP^{Sc}-specific antibody, mAb 8D5, which recognizes the N-terminal region comprising mouse PrP aa 31–39 (Masujin *et al.*, 2013). This mAb is expected to react with full-length PrP^{Sc} but not with the N-terminally truncated form of PrP^{Sc} that is generated by endogenous enzymes after PrP^{Sc} formation in the cells (Caughey *et al.*, 1991; Taraboulos *et al.*, 1992). The mAb 8D5 specifically immunoprecipitated PrP^{Sc} from brain homogenates of prion-infected animals, similar to other PrP^{Sc}-specific antibodies reported to date (Curin Serbec *et al.*, 2004; Horiuchi *et al.*, 2009; Korth *et al.*, 1997; Paramithiotis *et al.*, 2003; Ushiki-Kaku *et al.*, 2010). Of relevance is that the mAb 8D5 detected PrP^{Sc} in non-denatured histoblot and the cryosections of scrapie-infected mouse brains. This feature appeared to be useful for the immunocytochemical detection of PrP^{Sc}; thus, we attempted to use mAb 8D5 in combination with mAb 132 for PrP^{Sc}-specific detection.

In the current study, we prepared primary neuronal cultures from mouse cerebra with enrichment of neuronal population by antimitotic treatment and confirmed the prion propagation in the neurons. Then we compared PrP^{Sc} in immortalized cell lines and in primary neuronal cultures using PrP^{Sc}-specific double immunostaining.

Results

Detection of PrP^{Sc} in prion-infected immortalized cells by PrP^{Sc}-specific staining with mAbs 132 and 8D5

First we examined if mAb 8D5 reacts with PrP^{Sc} in prion-infected cells with or without pretreatment of cells with guanidine isothiocyanate (GdnSCN) (Fig. 1a). As expected, mAb 132 detected PrP^{Sc} in ScN2a-3-22L cells, which were a subclone of Neuro2a mouse neuroblastoma cell line (N2a-3) persistently infected with the 22L prion strain after pretreatment of cells with 5 M GdnSCN. Although fluorescence intensities were weaker than those by mAb 132, PrP^{Sc} signals were detected by mAb 8D5 in ScN2a-3-22L cells with or without GdnSCN pretreatment. Under the same condition of fluorescent image acquisition, mAb 8D5 did not show any specific fluorescent signals in prion-uninfected cells, demonstrating the PrP^{Sc}-specific detection.

To confirm the optimum condition of GdnSCN pretreatment for PrP^{Sc}-specific double immunostaining with mAbs 132 and 8D5, influence of the pretreatment on the PrP^{Sc} detection was analyzed using GT1 hypothalamic neuronal cell line (GT1-7) persistently infected with the 22L prion strain (ScGT1-7-22L) (Supplementary figure 1). The GdnSCN pretreatment did not enhance or degrade the reactivity of mAb 8D5 to PrP^{Sc} in ScGT1-7-22L cells so much. In contrast, the reactivity of mAb 132 drastically enhanced after the 5-min GdnSCN pretreatment. However, a longer GdnSCN pretreatment did not affect the reactivity of mAb 132. This result demonstrated that the 10-min pretreatment of cells with 5 M GdnSCN was optimum for the PrP^{Sc}-specific double immunostaining with mAbs 132 and 8D5, and thus, in

156 the following experiments, 10-min GdnSCN pretreatment was performed unless otherwise
157 specified.

158 Fig. 1(b) shows double immunofluorescent staining of PrP^{Sc} in ScN2a-3-22L cells using
159 mAbs 132 and 8D5. In ScN2a-3-22L cells, mAb 132 detected bright granular PrP^{Sc} signals at
160 perinuclear regions as previously described (Yamasaki *et al.*, 2012). In contrast, mAb 8D5
161 showed relatively faint granular PrP^{Sc} signals in ScN2a-3-22L cells (Fig. 1b, arrowheads).
162 Although some granular PrP^{Sc} signals detected by mAb 132 merged with those by mAb 8D5
163 (Fig. 1b, arrow), the majority of granular PrP^{Sc} stains by mAb 132 did not appear to be
164 co-localized with those by mAb 8D5. The results of the detailed colocalization analysis are
165 described later (see Fig. 6).

166 The same double immunofluorescent staining was carried out on ScGT1-7-22L cells.
167 MAb 132 showed perinuclear granular stains of PrP^{Sc}; however, the granular signals appeared
168 to be scattered to cytoplasm compared with ScN2a-3-22L cells (Fig. 1c). MAb 8D5 appeared
169 to detect greater number of PrP^{Sc} granules in ScGT1-7-22L cells than in ScN2a-3-22L cells.
170 PrP^{Sc} granular stains detected by mAb 8D5 were scattered to the cytoplasm and some
171 granules with intense fluorescence were observed at the peripheral region of cytoplasm,
172 possibly proximate the plasma membranes (Fig. 1c, arrowheads). PrP^{Sc} detected by mAbs 132
173 and 8D5 was partly but not extensively merged (Fig. 1c, arrows).

174

175 ***Neuron-enriched primary cultures from mouse cerebra***

176 Cells isolated from the cerebra of mouse embryos were abundant in neurons and
177 contained a few glial cells (Fig. 2b, e.g., 7 days in vitro [div], cytosine arabinoside [Ara-C]
178 [−]). However, in the absence of Ara-C, glial fibrillary acidic protein (GFAP)-positive

179 astrocytes readily increased by 14 div (Fig. 2b). Ara-C treatment at 0.25 μM from 4 to 7 div
180 and following treatment at 0.125 μM from 7 to 11 div successfully suppressed the appearance
181 of GFAP-positive astrocytes up to 28 div; only a few astrocytes were found in Ara-C-treated
182 cultures until 28 div. The result of GFAP expression in immunoblot analysis also
183 demonstrated the successful reduction of astrocytes (Fig. 2c). A neuron-specific protein,
184 βIII-tubulin, was detected from primary neuronal cultures in the presence or absence of Ara-C
185 by immunoblot analysis (Fig. 2c). Lower levels of GFAP but higher levels of βIII-tubulin in
186 Ara-C-treated primary neuronal cultures at each time point also indicated that the Ara-C
187 treatment by the indicated schedule securely resulted in the enrichment of neurons in the
188 primary neuronal cultures. We designate this culture as primary cerebral neurons (CNs) in the
189 description below.
190
191 ***PrP^{Sc} generation in CNs***
192 The CNs at 7 div were exposed to microsomes as described in the section of Materials
193 and Methods. Four days after the exposure, the medium was replaced with fresh, Ara-C-free
194 Neuronal Medium to remove inocula (Fig. 2a). The CNs at 0, 7, 14, 21, 28, and 35 days post
195 infection (dpi) were subjected to immunoblot analysis for proteinase K (PK)-resistant PrP^{Sc}
196 (PrP-res) detection (Fig. 3a). PrP-res was detected in cells exposed to three different prion
197 strains from at least 7 dpi. In CNs infected with 22L or Chandler strain, PrP-res levels
198 increased up to 21 dpi, demonstrating prion propagation. In Obihiro strain-infected CNs, the
199 PrP-res level was lower than CNs infected with other two prion strains. No PrP-res was
200 detected in mock-infected CNs. Figure 3(b) shows PrP^{Sc}-specific immunostaining using mAb
201 132. PrP^{Sc} signals were observed around cell bodies and neurites in prion-infected CNs from

7 dpi but not in mock-infected CNs. The PrP^{Sc} stains per cell appeared to gradually increase up to 21 dpi, and most CNs were positive for PrP^{Sc} at 14 dpi (data not shown). The granular PrP^{Sc} stains at perinuclear regions, as observed in ScN2a-3-22L cells and N2a-3 cells persistently infected with the Chandler prion strain (ScN2a-3-Ch), were scarcely observed in prion-infected CNs. However, string-like stains around the edges of cell bodies and neurites were evident during the later stage of infection (Fig. 3b, arrows).

PrP^{Sc}-specific double immunostaining of prion-infected CNs using mAbs 132 and 8D5

To characterize the string-like PrP^{Sc} stains in prion-infected CNs that were detected by mAb 132 (Fig. 3b), PrP^{Sc}-specific double immiunostaining was performed with mAbs 132 and 8D5. In 22L or Chandler strain-infected CNs (at 14 dpi), string-like PrP^{Sc} stains (Fig. 4, closed arrows) were detected by both mAbs 132 and 8D5, and they were partly merged (Fig. 4, arrowheads). In addition to string-like PrP^{Sc} stains, granular PrP^{Sc} stains single positive for mAb 132 were observed at neurites but hardly at somas (Fig. 4, open arrows). The string-like PrP^{Sc} stains were evident but less obvious in Obihiro strain-infected CNs compared with 22L or Chandler strain-infected CNs.

Since PrP^{Sc} stains in prion-infected CNs appeared at the plasma membranes or extracellular space, living CNs were incubated with Alexa Fluor 488-conjugated mAb 8D5 and subjected to microscopic examination to confirm whether the string-like PrP^{Sc} is present on the cell surface (Fig. 5). The CNs infected with 22L, Chandler, or Obihiro strains at 14 dpi were incubated with mAb 8D5 and were directly subjected to microscopic observation without fixation, permeabilization or denaturation. String-like and granular-like stains of PrP^{Sc} similar to those in fixed cells (Fig. 4) were observed in CNs infected with prions,

225 demonstrating the presence of PrP^{Sc} on the cell surface (Fig. 5). The result also indicated that
226 certain population of PrP^{Sc} on the cell surface of CNs possesses the N-terminal region that is
227 recognized with mAb 8D5. PrP^{Sc} stains were also clearly detected on the surface of
228 ScGT1-7-22L cells but not obvious on the surface of ScN2a3-22L cells (Supplementary
229 figure 2).
230
231
232 ***Colocalization of PrP^{Sc} detected by mAbs 132 and 8D5 in immortalized cells and CNs***
233 PrP^{Sc}-specific double staining revealed differences in immunoreactivity of PrP^{Sc}
234 between immortalized cell lines and CNs; PrP^{Sc} positive for mAb 8D5 was more apparent in
235 CNs infected with the 22L strain than in ScN2a-3-22L cells. To assess the differences in
236 detail, quantitative analysis of PrP^{Sc} populations was performed based on the reactivity with
237 mAbs 132 and 8D5 (Fig. 6). In ScN2a-3-22L cells, only 6.6 % of the total PrP^{Sc} signals in
238 cells were positive for both mAbs (Fig. 6b). In contrast, the proportion of double-positive
239 PrP^{Sc} appeared to be higher in ScGT1-7-22L cells and prion-infected CNs than in
240 ScN2a-3-22L cells; 18.9% in ScGT1-7-22L cells and 13.5%–24.9% in CNs infected with
241 three different prion strains. In ScN2a-3-22L cells, 92.3% of PrP^{Sc} were positive for mAb 132
242 (Fig. 6c, red and yellow bars), whereas only 14.3% were positive for mAb 8D5 (Fig. 6c, green
243 and yellow bars). The proportion of PrP^{Sc} population detected by mAb 132 in CNs infected
244 with the 22L prion strain (78.9%) was significantly lower than that in ScN2a-3-22L cells (Fig.
245 6c, $p< 0.05$). Conversely, nearly half of PrP^{Sc} was positive for mAb 8D5 in CNs infected with
246 22L prion strain (46.0%), which was significantly higher than that in ScN2a-3-22L cells (Fig.
247 6c, $p<0.01$). Although no difference was observed in the proportion of mAb 132-positive

248 PrP^{Sc} between ScN2a-3-22L and ScGT1-7-22L cells (88.8%) or between ScGT1-7-22L and
249 CNs infected with the 22L prion strain, the proportion of mAb 8D5-positive PrP^{Sc} in
250 ScGT1-7-22L cells (30.2%) was significantly higher than in ScN2a-3-22L cells, but lower
251 than in CNs infected with 22L prion strain (Fig. 6c, $p< 0.05$).
252
253 ***Biochemical properties of PrP molecules in cells***
254 PrP^{Sc}-specific immunofluorescence staining revealed differences in staining pattern of
255 PrP^{Sc} among cell types, particularly between ScN2a-3-22L cells and ScGT1-7-22L cells or
256 CNs infected with the 22L strain. To address the differences, we performed immunoblotting
257 to detect total PrP (both PK-sensitive and PK-resistant PrP) without PK treatment (Fig. 7a).
258 The level of the full length PrP was apparently lower in ScN2a-3-22L cells than in N2a-3
259 cells. In contrast, GT1-7 and ScGT1-7-22L cells, and CNs and CNs infected with the 22L
260 strain had comparable amount of full length PrP. These results suggest that ScN2a-3-22L cells
261 have a higher N-terminal processing activity and that the cells produce the N-terminal
262 truncated PrP^{Sc} that lacks the epitope for mAb 8D5. This idea is consistent with the results of
263 PrP^{Sc}-specific immunofluorescence staining: PrP^{Sc} stains positive for mAb 132 were more
264 evident than those positive for mAb 8D5 in ScN2a3-22L cells (Fig. 1a). By contrast, mAb
265 8D5 seemed to detect PrP^{Sc} efficiently in ScGT1-7-22L cells (Fig. 1d) and CNs infected with
266 the 22L strain (Figs 4 and 5).
267 To analyze PrP^{Sc} recognized by mAb 8D5, PrP^{Sc} was immunoprecipitated from GT1-7
268 cells with mAb 8D5 and then subjected to immunoblotting with mAb 110, which recognizes
269 the epitope in the octapeptide repeat region (Fig. 7b). PrP bands were detected only in the
270 precipitates from ScGT1-7-22L cells, demonstrating the PrP^{Sc}-specificity of

immunoprecipitation. The mAb 110 detected broad bands around 36 and 30 kDa as well as bands lower than 25 kDa. The 36 kDa broad band corresponds to full length PrP^{Sc}, indicating the existence of full length PrP^{Sc} on the cell surface. Regarding broad bands around 30 kDa and band with approx. 25 kDa, it is difficult to conclude whether these bands represent mono- or non-glycosylated full length PrP^{Sc} or di- or mono-glycosylated N-terminal truncated PrP^{Sc} that were co-precipitated with full length PrP^{Sc} during the immunoprecipitaion. However, no immunoreactive bands were observed below 15 kDa, even around the running front (data not shown). This suggests that PrP molecule possessing the extreme N-terminus but lacking the C-terminal core region will be negligible even if it exists.

Discussion

The mAb 8D5 recognizes the epitope composed of the extreme N-terminus of PrP (aa 31–39) (Masujin et al., 2013). It is well known that the N-terminus of PrP is partly digested by cellular events (Caughey *et al.*, 1991; Chen *et al.*, 1995). MAb 132 recognizes the epitope composed of aa 119–127 of PrP that remains in the C-terminal core fragment of PrP^{Sc}, possibly analogous to the C2 fragment (Chen *et al.*, 1995). Thus, PrP^{Sc}-specific double staining using the mAbs is expected to provide more precise information on intracellular localization of PrP^{Sc}. Indeed, PrP^{Sc} stains with mAb 132 were not always merged with those by mAb 8D5, indicating that the double staining detected greater number of PrP^{Sc} molecules than single-staining (Figs. 1, 4, and 6). The mAb 132-positive but mAb 8D5-negative PrP^{Sc} signals may represent the N-terminally truncated PrP^{Sc} molecules. Unexpectedly, however, certain PrP^{Sc} was mAb 8D5 positive but mAb 132 negative in the double staining. The

294 reactivity implies the existence of PrP^{Sc} composed only of the N-terminal portion of the PrP
295 molecule; however, this is unlikely. The N-terminal portion of PrP^{Sc} is easily digested by PK
296 treatment, indicating that the N-terminal portion locates the accessible surface of PrP^{Sc}
297 oligomers/aggregates. Thus, anti-PrP antibodies may be able to more readily access the
298 N-terminal portion than the C-terminal portion of PrP^{Sc}. The antibody molecule is nearly
299 5-fold larger than a single PrP molecule; therefore, once mAb 8D5 binds to PrP^{Sc}, it may
300 disturb the binding of mAb 132 to the epitope even on the neighboring PrP molecule of PrP^{Sc}
301 oligomers by steric hindrance. Indeed, ScN2a-3-22L cells were stained with Alexa Fluor
302 488-labeded mAb 132 and Alexa Flour 647-labeled mAb 132 simultaneously, 65.7 ± 2.3 % of
303 Alexa 488-labeled PrP^{Sc} stains were also stained with Alexa Flour-647. These factors will
304 affect the interpretation of the results; nevertheless, PrP^{Sc}-specific multiple staining using two
305 or more antibodies, as shown here, is one of the effective approaches for precise
306 understanding of intracellular localization of PrP^{Sc} and the mechanism for prion propagation.
307 Although PrP^{Sc} has been reported to be detected on the cell surface of prion-infected
308 immortalized neuronal cells (Goold *et al.*, 2011; Rouvinski *et al.*, 2014; Yamasaki *et al.*,
309 2012), cell biological studies using immortalized cell lines strongly suggested that the PrP^{Sc}
310 formation takes place at cellular compartments along with the endocytic recycling pathway
311 such as the endocytic recycling compartments, or those along with the endo-lysosomal
312 pathway such as multivesicular bodies (Beranger *et al.*, 2002; Borchelt *et al.*, 1992;
313 Marijanovic *et al.*, 2009; Pimpinelli *et al.*, 2005; Veith *et al.*, 2009; Yamasaki *et al.*, 2014a;
314 Yamasaki *et al.*, 2012). In contrast, ultrastructural analyses using brains of prion-infected
315 mice and hamsters frequently identified PrP^{Sc} at the plasma membranes and less frequently at
316 synapses and compartments of the endo-lysosomal system (Arnold *et al.*, 1995; Fournier *et al.*,

2000; Godsave *et al.*, 2008). Recently, Godsave et al. reported that in RML strain-infected mouse brains, the majority of PrP^{Sc} clusters were detected at the plasma membranes, including membrane invaginations and the site of cell-to-cell contact, whereas in the other subcellular regions such as synapses and intracellular vesicles, PrP^{Sc} clusters were detected only occasionally by immuno-electron microscopic examination using an antibody that recognizes the N-terminal region of PrP (Godsave *et al.*, 2013). The authors believed that PrP^{Sc} detected by the anti-PrP N-terminus mAb Saf32 included nascent full-length PrP^{Sc}, as the N-terminal region tends to be processed after generation of PrP^{Sc} (Caughey *et al.*, 1991; Taraboulos *et al.*, 1992). Considered collectively, ultrastructural studies suggest the plasma membranes as the primary site for PrP^{Sc} formation. In the current study, we found that morphology and cellular localization of PrP^{Sc} differ in immortalized cell lines and CNs: in N2a-3 and GT1-7 cells infected with 22L prion strain (Fig. 1b and c), PrP^{Sc} was mainly detected as granule-like stains at the perinuclear regions, as previously reported (Schatzl *et al.*, 1997; Yamasaki *et al.*, 2012), whereas in CNs infected with the 22L- or Chandler strain, PrP^{Sc} was detected as unique string-like stains, possibly on the cell surface; however, a few were detected in the cytoplasm (Figs. 4 and 5). Rouvinski et al. recently reported that in addition to granule-like PrP^{Sc} stains in the cytoplasm, strings-like PrP^{Sc} stains were detected on the surface of 22L or RML prion strain-infected GT1 cells. The string-like PrP^{Sc} was detected by anti-PrP antibodies recognizing the N-terminal part of PrP and was demonstrated as glycosylphosphatidylinositol-anchored PrP^{Sc} amyloids (Rouvinski *et al.*, 2014). However, compared with the results by Rouvinski et al, string-like PrP^{Sc} stains were predominantly observed on the surface of CNs; however, a few intracellular granule-like PrP^{Sc} stains were observed in the CNs (Fig. 4). Taken together, the differences in PrP^{Sc} stains suggest that the

mechanism of PrP^{Sc} formation in immortalized cell lines may not be exactly the same as that in CNs. Interestingly, Rouvinski et al. also detected string-like PrP^{Sc} stains in brains of scrapie-infected mice (Rouvinski *et al.*, 2014). Furthermore, filamentous depositions of PrP^{Sc} were frequently observed in the white matter of patients with inherited prion diseases (Reiniger *et al.*, 2013) and in the neuropils of the 22L prion strain-infected cerebellar slices (Wolf *et al.*, 2015). In addition, it was reported that PrP^{Sc} accumulates predominantly as unprocessed forms in brain tissues and in the primary cultured cerebellar granule neurons (Dron *et al.*, 2010). Since PrP^{Sc} detected by mAb 8D5 is expected to be a full-length PrP^{Sc}, therefore, the morphological, and locational as well as biochemical similarities of PrP^{Sc} stains in prion-infected CNs and brains of patients or animals affected by prion diseases suggest that the mechanism of PrP^{Sc} formation in CNs is, at least to some extent, similar to that in neurons in CNS.

In the previous reports using prion-infected primary cultured neurons, antimitotics were used throughout the culture period to suppress the growth of astrocytes (Carimalo *et al.*, 2005; Cronier *et al.*, 2007; Hannaoui *et al.*, 2013), and some of them confirmed the neuronal predominance with astrocytes at 4%–5% of the cellular composition at an early stage (Cronier *et al.*, 2004). However, antimitotics will be harmful to neurons depending on concentrations and the period of treatment. In the current study, we showed that temporary treatment of Ara-C successfully reduced astrocyte proliferation and enabled us to keep CNs up to 4 weeks after prion inoculation (Fig. 2). The CNs supported prion propagation with various prion strains including Obihiro strain that is not propagated well in N2a-3 and GT1-7 cells (Uryu *et al.*, 2007). Difference in PrP^{Sc} stains in CNs infected with Obihiro strain (Fig. 4) may be partly due to a biochemical difference of PrP^{Sc} among prion strains. Furthermore,

363 PrP^{Sc}-specific double staining using mAbs 132 and 8D5 suggested that CNs share the same
364 mechanism for prion propagation with neurons in central nervous system. The presence of
365 PrP^{Sc} at neurites in the CNs is of interest, because neurodegeneration in prion diseases is
366 reported to be initiated at axonal terminals (Gray *et al.*, 2009), dendrites (Fuhrmann *et al.*,
367 2007) or synapses (Jeffrey *et al.*, 2000) rather than at the soma of neurons. Thus,
368 neuron-enriched primary cultures used in the current study will be an invaluable *ex vivo*
369 model for analyzing the mechanism of neurodegeneration caused by prion infection.
370
371
372 ***Materials and methods***
373 ***Antibodies***
374 MAbs 31C6, 132, and 8D5 that recognize epitopes consisting of mouse PrP aa 143–149,
375 119–127 (Kim *et al.*, 2004), and 31–39 (Masujin *et al.*, 2013), respectively, were used. MAb
376 110 that recognizes the epitope in the octapeptide repeat of PrP, PHGGGWG, at aa 59–65 and
377 83–89 was also used (Kim et al., 2004). For direct immunofluorescent staining of PrP^{Sc},
378 mAbs 132 and 8D5 were conjugated with Alexa Fluor 647 and 488, respectively, using Alexa
379 Fluor Carboxylic Acid Succinimidyl Ester mixed isomers (Life Technologies). The following
380 antibodies were also used for IFA or immunoblot analysis: anti-microtubule-associated
381 protein 2 (MAP2) chicken polyclonal antibodies (pAbs) (Abcam, ab5392), anti-GFAP rabbit
382 pAbs (Dako, 0334), and anti-βIII-tubulin rabbit pAbs (Abcam, ab18207). MAb P2-284
383 against feline panleukopenia virus was used as an isotype control antibody (Horiuchi *et al.*,
384 1997).
385

Cell lines

A subclone of the Neuro2a mouse neuroblastoma cell line, N2a-3 (Uryu *et al.*, 2007), and a subclone of the GT1 hypothalamic neuronal cell line, GT1-7 (Schatzl *et al.*, 1997), were used. ScN2a-3-22L (Nakamitsu *et al.*, 2010), ScN2a-3-Ch (Uryu et al., 2007), and GT1-7 persistently infected with the 22L prion strain (ScGT1-7-22L) (Yamasaki *et al.*, 2012) were used as prion-infected cells. Those cells were cultured as described previously (Uryu *et al.*, 2007; Yamasaki *et al.*, 2012) and used at passage history between 5 and 30.

Primary neuronal cell culture

Chamber covers of 8-well configurations (Matsunami), 96-well μ-plates (ibidi), and 24-well plastic culture plates were coated with 20 μg poly-L-lysine (Sigma) ml^{-1} in PBS and settled overnight at room temperature (RT). After washing twice with sterilized de-ionized water, Neurobasal Medium (Life Technologies) containing 1 × B-27 Supplement (Life Technologies) and 6 mM GlutaMAX (Life Technologies) (hereafter Neuronal Medium) was added into each well and the plates were kept at 37 °C in 5% CO_2 atmosphere until use.

Primary neuronal cell cultures were prepared from ICR mouse embryos of embryonic day 14 (pregnant mice were purchased from Japan Clea Inc.). The experimental procedures have been approved by the Institutional Animal Care and Use Committee at Hokkaido University (No. 13-0141). The diencephalon, mesencephalon, medulla oblongata, and cerebellum were removed from embryonic brains, and the olfactory bulb, hippocampi, and meninges were resected under a stereo microscope. The remaining tissues including cerebral cortices were digested using the Neural Tissue Dissociation Kit (P) (Miltenyi Biotec) according to the manufacturer's instructions but modified by enzymatic reactions being

409 performed on ice. Tissues were dispersed by gentle pipetting and filtrated through cell strainer
410 with 100 μm nylon mesh (Corning). The cells were collected by centrifugation at 300 × g for
411 5 min at 4 °C. All procedures described above were performed using ice-cold Hank's
412 Balanced Salt Solution (Sigma) containing 100 μM HEPES (Life Technologies) and 10 μM
413 sodium pyruvate (Life Technologies). Cells were resuspended in the Neuronal Medium and
414 were plated at a density of 1.0×10^5 cells on poly-L-lysine pre-coated glass or plastic plates
415 cm^{-2}. Half of the culture medium was replaced with fresh Neuronal Medium every week. To
416 inhibit astrocyte proliferation, Ara-C (Sigma) was added at a final concentration of 0.25 μM
417 to cultures at 4 div. The Ara-C concentration was reduced by half accompanying the prion
418 infection at 7 div, following which cultures were maintained in Ara-C free Neuronal Medium
419 after 11 div (see Fig.2a).

420 Inocula containing prions were prepared from brains of mice infected with the 22L,
421 Chandler, or Obihiro prion strains (all are mouse-adapted scrapie prions) at the terminal stage
422 of the disease, and brains of age-matched, uninfected ICR mice were used as a control. The
423 brains were homogenized in sterile PBS at a concentration of 10% w/v. The homogenates
424 were sonicated for 3.5 min and centrifuged at 3,000 × g for 10 min at 4 °C. The resulting
425 supernatant was centrifuged at 100,000 × g for 60 min at 4 °C, and the pellet containing
426 microsomes was suspended in sterile PBS. The amount of PrP-res in the material was
427 quantified by immunoblot analysis using purified PrP-res as a standard (Yamasaki *et al.*,
428 2014a). Primary neuronal cell cultures at 7 div were exposed to the inocula equivalent to 5 ng
429 of PrP-res per 1.0×10^5 cells by replacement of half of medium in each well. The medium
430 was completely replaced by fresh Neuronal Medium at 4 dpi that corresponds to 11 div (see
431 Fig. 2a).

Immunoblot analysis

Neurons cultured on 24-well plastic plates were washed with PBS and treated with 200 μl of lysis buffer (0.5% TritonX-100, 0.5% sodium deoxycholate, 150 mM NaCl, 5 mM EDTA, and 10 mM Tris-HCl [pH 7.5]) for 30 min at 4 °C. The cells were then lysed by one cycle of freeze-thaw and subsequent pipetting. The lysate was clarified by centrifugation at 2,000 × g for 5 min at 4 °C. Protein concentration of the lysates was measured using a DC protein assay kit (Bio-Rad) and adjusted to 0.3 mg ml^{-1}. For detection of PrP-res, PK were added to the lysates at a final concentration of 4% to the amount of total protein and incubated at 37 °C for 20 min. PK digestion was terminated by the addition of Pefabloc (Roche) to 1 mM, and the lysates were then treated with 50 μg DNase I ml^{-1} at RT for 15 min. Precipitation of PrP-res by phosphotungstic acid (PTA) and following SDS-PAGE, Western transfer, and chemiluminescence detection were carried out as described elsewhere (Shindoh *et al.*, 2009; Uryu *et al.*, 2007). For detection of GFAP and βIII-tubulin, the procedures from PK digestion to PTA precipitation were omitted, and 2 μg of total protein was loaded onto each lane.

Immunoprecipitation

GT1-7 cells grown on 10 cm dish at approximately 80% confluence were used. After washing cells gently with cold PBS, cells were incubated with 15 μg of mAb at 4 °C for 1 h. After washing the cells three times, cells were collected by cell scraper and lysed with PBS containing 1% Zwittergent 3-14 (Calbiochem) and 1× cOmplete Protease Inhibitor Cocktail (Roche). The cell lysates were clarified by centrifugation at 500 × g for 10 min, the resulting supernatants (50 μg protein equivalent) were mixed with Dynabeads Protein G (Milteny) that

455 were blocked with 1% I-BLOCK (Applied Biosystems) and 20 % N-101 (NOF Cooperation)
456 and pre-incubated with anti-mouse IgG Fc-specific goat IgG. Mixtures were incubated at 4 °C
457 for 90 min with constant rotation and then the beads were washed five times with PBS
458 containing 1% Tween 20 using magnetic separator. Immunoprecipitates were eluted with the
459 SDS sample buffer by boiling for 10 min and subjected to immunoblotting. Blots were probed
460 with mAb 110 labeled with horseradish peroxidase (Horiuchi *et al.*, 2009).
461
462 ***IFA***
463 Primary neurons grown on 8-well chamber covers or 96-well μ-plates, and N2a-3 or
464 GT1-7 cells grown on 8-well Lab-Tek II chambered coverglass (Nunc) were fixed with PBS
465 containing 4% paraformaldehyde and 4% sucrose at RT for 10 min. Subsequently, procedures
466 for IFA were carried out as described previously (Yamasaki *et al.*, 2014a; Yamasaki *et al.*,
467 2014b). In some cases, mAbs conjugated with Alexa Fluor fluorescence dye were used for the
468 direct immunostaining of PrP^{Sc}.
469 For the detection of PrP^{Sc} on the cell surface, cells were gently rinsed with prewarmed
470 sterile PBS and incubated with the Neuronal Medium containing 1 μg Alexa Fluor
471 488-conjugated mAb 8D5 ml^{-1} at 37 °C for 1 h. The cells were gently rinsed and covered with
472 PBS for the microscopic examination.
473
474 ***Colocalization analysis***
475 3D fluorescent images were constructed from the Z-stack images and surfaces. The 3D
476 bodies that were positive for each antibody, were identified by Imaris software version 7.6.1.
477 (Bitplane). The minimum unit of the surfaces, termed voxel(s), which was positive for each

antibody, was counted for colocalization statistics.

Acknowledgments

This work was supported by a Grant-in-Aid for Science Research (A) (grant no. 15H02475), a grant from the Program for Leading Graduate Schools (F01), and the Japan Initiative for Global Research Network on Infectious Diseases (J-GRID), from the Ministry of Education, Culture, Sports, Science, and Technology, Japan. This work was also supported by grants for TSE research (H26-Shokuhin-Ippan-003) and Research on Measures for Intractable Diseases from the Ministry of Health, Labour and Welfare of Japan. We thank Zensho Co., Ltd, for the BSL3 facility. This work was also supported in part by the Intramural Research Program of the NIAID.

492 ***References***

493

494 **Arnold, J. E., Tipler, C., Laszlo, L., Hope, J., Landon, M. & Mayer, R. J. (1995).** The
495 abnormal isoform of the prion protein accumulates in late-endosome-like organelles in
496 scrapie-infected mouse brain. *J Pathol* **176**, 403-411.

497 **Beranger, F., Mange, A., Goud, B. & Lehmann, S. (2002).** Stimulation of PrP(C)
498 retrograde transport toward the endoplasmic reticulum increases accumulation of
499 PrP(Sc) in prion-infected cells. *J Biol Chem* **277**, 38972-38977.

500 **Borchelt, D. R., Taraboulos, A. & Prusiner, S. B. (1992).** Evidence for synthesis of scrapie
501 prion proteins in the endocytic pathway. *J Biol Chem* **267**, 16188-16199.

502 **Carimalo, J., Cronier, S., Petit, G., Peyrin, J. M., Boukhtouche, F., Arbez, N.,**
503 **Lemaigre-Dubreuil, Y., Brugg, B. & Miquel, M. C. (2005).** Activation of the
504 JNK-c-Jun pathway during the early phase of neuronal apoptosis induced by
505 PrP106-126 and prion infection. *Eur J Neurosci* **21**, 2311-2319.

506 **Caughey, B. & Raymond, G. J. (1991).** The scrapie-associated form of PrP is made from a
507 cell surface precursor that is both protease- and phospholipase-sensitive. *J Biol Chem*
508 **266**, 18217-18223.

509 **Caughey, B., Raymond, G. J., Ernst, D. & Race, R. E. (1991).** N-terminal truncation of the
510 scrapie-associated form of PrP by lysosomal protease(s): implications regarding the
511 site of conversion of PrP to the protease-resistant state. *J Virol* **65**, 6597-6603.

512 **Chen, S. G., Teplow, D. B., Parchi, P., Teller, J. K., Gambetti, P. & Autilio-Gambetti, L.**
513 **(1995).** Truncated forms of the human prion protein in normal brain and in prion
514 diseases. *J Biol Chem* **270**, 19173-19180.

515 **Cronier, S., Beringue, V., Bellon, A., Peyrin, J. M. & Laude, H. (2007).** Prion strain- and
516 species-dependent effects of antiprion molecules in primary neuronal cultures. *J Virol*
517 **81**, 13794-13800.

518 **Cronier, S., Laude, H. & Peyrin, J. M. (2004).** Prions can infect primary cultured neurons
519 and astrocytes and promote neuronal cell death. *Proc Natl Acad Sci U S A* **101**,
520 12271-12276.

521 **Curin Serbec, V., Bresjanac, M., Popovic, M., Pretnar Hartman, K., Galvani, V.,**
522 **Rupreht, R., Cernilec, M., Vranac, T., Hafner, I. & Jerala, R. (2004).** Monoclonal
523 antibody against a peptide of human prion protein discriminates between
524 Creutzfeldt-Jacob's disease-affected and normal brain tissue. *J Biol Chem* **279**,
525 3694-3698.

526 **Dron, M., Moudjou, M., Chapuis, J., Salamat, M. K., Bernard, J., Cronier, S., Langevin,**
527 **C. & Laude, H. (2010).** Endogenous proteolytic cleavage of disease-associated prion
528 protein to produce C2 fragments is strongly cell- and tissue-dependent. *J Biol Chem*

285, 10252-10264.

Fournier, J. G., Escaig-Haye, F. & Grigoriev, V. (2000). Ultrastructural localization of prion proteins: physiological and pathological implications. *Microsc Res Tech* **50**, 76-88.

Fuhrmann, M., Mitteregger, G., Kretzschmar, H. & Herms, J. (2007). Dendritic pathology in prion disease starts at the synaptic spine. *J Neurosci* **27**, 6224-6233.

Godsave, S. F., Wille, H., Kujala, P., Latawiec, D., DeArmond, S. J., Serban, A., Prusiner, S. B. & Peters, P. J. (2008). Cryo-immunogold electron microscopy for prions: toward identification of a conversion site. *J Neurosci* **28**, 12489-12499.

Godsave, S. F., Wille, H., Pierson, J., Prusiner, S. B. & Peters, P. J. (2013). Plasma membrane invaginations containing clusters of full-length PrPSc are an early form of prion-associated neuropathology in vivo. *Neurobiol Aging* **34**, 1621-1631.

Goold, R., Rabbanian, S., Sutton, L., Andre, R., Arora, P., Moonga, J., Clarke, A. R., Schiavo, G., Jat, P., Collinge, J. & Tabrizi, S. J. (2011). Rapid cell-surface prion protein conversion revealed using a novel cell system. *Nat Commun* **2**, 281.

Gray, B. C., Siskova, Z., Perry, V. H. & O'Connor, V. (2009). Selective presynaptic degeneration in the synaptopathy associated with ME7-induced hippocampal pathology. *Neurobiol Dis* **35**, 63-74.

Hannaoui, S., Maatouk, L., Privat, N., Levavasseur, E., Faucheux, B. A. & Haik, S. (2013). Prion propagation and toxicity occur in vitro with two-phase kinetics specific to strain and neuronal type. *J Virol* **87**, 2535-2548.

Horiuchi, M., Karino, A., Furuoka, H., Ishiguro, N., Kimura, K. & Shinagawa, M. (2009). Generation of monoclonal antibody that distinguishes PrPSc from PrPC and neutralizes prion infectivity. *Virology* **394**, 200-207.

Horiuchi, M., Mochizuki, M., Ishiguro, N., Nagasawa, H. & Shinagawa, M. (1997). Epitope mapping of a monoclonal antibody specific to feline panleukopenia virus and mink enteritis virus. *J Vet Med Sci* **59**, 133-136.

Jeffrey, M., Goodsir, C. M., Bruce, M., McBride, P. A., Scott, J. R. & Halliday, W. G. (1994). Correlative light and electron microscopy studies of PrP localisation in 87V scrapie. *Brain Res* **656**, 329-343.

Jeffrey, M., Goodsir, C. M., Bruce, M. E., McBride, P. A., Scott, J. R. & Halliday, W. G. (1992). Infection specific prion protein (PrP) accumulates on neuronal plasmalemma in scrapie infected mice. *Neurosci Lett* **147**, 106-109.

Jeffrey, M., Halliday, W. G., Bell, J., Johnston, A. R., MacLeod, N. K., Ingham, C., Sayers, A. R., Brown, D. A. & Fraser, J. R. (2000). Synapse loss associated with abnormal PrP precedes neuronal degeneration in the scrapie-infected murine hippocampus. *Neuropathol Appl Neurobiol* **26**, 41-54.

Kim, C. L., Umetani, A., Matsui, T., Ishiguro, N., Shinagawa, M. & Horiuchi, M. (2004).

Antigenic characterization of an abnormal isoform of prion protein using a new diverse panel of monoclonal antibodies. *Virology* **320**, 40-51.

Korth, C., Stierli, B., Streit, P., Moser, M., Schaller, O., Fischer, R., Schulz-Schaeffer, W., Kretzschmar, H., Raeber, A., Braun, U., Ehrensperger, F., Hornemann, S., Glockshuber, R., Riek, R., Billeter, M., Wuthrich, K. & Oesch, B. (1997). Prion (PrPSc)-specific epitope defined by a monoclonal antibody. *Nature* **390**, 74-77.

Mallucci, G., Dickinson, A., Linehan, J., Klohn, P. C., Brandner, S. & Collinge, J. (2003). Depleting neuronal PrP in prion infection prevents disease and reverses spongiosis. *Science* **302**, 871-874.

Marijanovic, Z., Caputo, A., Campana, V. & Zurzolo, C. (2009). Identification of an intracellular site of prion conversion. *PLoS Pathog* **5**, e1000426.

Masujin, K., Kaku-Ushiki, Y., Miwa, R., Okada, H., Shimizu, Y., Kasai, K., Matsuura, Y. & Yokoyama, T. (2013). The N-terminal sequence of prion protein consists an epitope specific to the abnormal isoform of prion protein (PrP(Sc)). *PLoS One* **8**, e58013.

Nakamitsu, S., Kurokawa, A., Yamasaki, T., Uryu, M., Hasebe, R. & Horiuchi, M. (2010). Cell density-dependent increase in the level of protease-resistant prion protein in prion-infected Neuro2a mouse neuroblastoma cells. *J Gen Virol* **91**, 563-569.

Naslavsky, N., Stein, R., Yanai, A., Friedlander, G. & Taraboulos, A. (1997). Characterization of detergent-insoluble complexes containing the cellular prion protein and its scrapie isoform. *J Biol Chem* **272**, 6324-6331.

Paramithiotis, E., Pinard, M., Lawton, T., LaBoissiere, S., Leathers, V. L., Zou, W. Q., Estey, L. A., Lamontagne, J., Lehto, M. T., Kondejewski, L. H., Francoeur, G. P., Papadopoulos, M., Haghighat, A., Spatz, S. J., Head, M., Will, R., Ironside, J., O'Rourke, K., Tonelli, Q., Ledebur, H. C., Chakrabartty, A. & Cashman, N. R. (2003). A prion protein epitope selective for the pathologically misfolded conformation. *Nat Med* **9**, 893-899.

Pimpinelli, F., Lehmann, S. & Maridonneau-Parini, I. (2005). The scrapie prion protein is present in flotillin-1-positive vesicles in central- but not peripheral-derived neuronal cell lines. *Eur J Neurosci* **21**, 2063-2072.

Prusiner, S. B. (1998). Prions. *Proc Natl Acad Sci U S A* **95**, 13363-13383.

Reiniger, L., Mirabile, I., Lukic, A., Wadsworth, J. D., Linehan, J. M., Groves, M., Lowe, J., Druyeh, R., Rudge, P., Collinge, J., Mead, S. & Brandner, S. (2013). Filamentous white matter prion protein deposition is a distinctive feature of multiple inherited prion diseases. *Acta Neuropathol Commun* **1**, 8.

Rouvinski, A., Karniely, S., Kounin, M., Moussa, S., Goldberg, M. D., Warburg, G., Lyakhovetsky, R., Papy-Garcia, D., Kutzsche, J., Korth, C., Carlson, G. A., Godsave, S. F., Peters, P. J., Luhr, K., Kristensson, K. & Taraboulos, A. (2014).

Live imaging of prions reveals nascent PrPSc in cell-surface, raft-associated amyloid strings and webs. *J Cell Biol* **204**, 423-441.

Sakai, K., Hasebe, R., Takahashi, Y., Song, C. H., Suzuki, A., Yamasaki, T. & Horiuchi, M. (2013). Absence of CD14 delays progression of prion diseases accompanied by increased microglial activation. *J Virol* **87**, 13433-13445.

Schatzl, H. M., Laszlo, L., Holtzman, D. M., Tatzelt, J., DeArmond, S. J., Weiner, R. I., Mobley, W. C. & Prusiner, S. B. (1997). A hypothalamic neuronal cell line persistently infected with scrapie prions exhibits apoptosis. *J Virol* **71**, 8821-8831.

Shindoh, R., Kim, C. L., Song, C. H., Hasebe, R. & Horiuchi, M. (2009). The region approximately between amino acids 81 and 137 of proteinase K-resistant PrPSc is critical for the infectivity of the Chandler prion strain. *J Virol* **83**, 3852-3860.

Taraboulos, A., Raeber, A. J., Borchelt, D. R., Serban, D. & Prusiner, S. B. (1992). Synthesis and trafficking of prion proteins in cultured cells. *Mol Biol Cell* **3**, 851-863.

Taraboulos, A., Serban, D. & Prusiner, S. B. (1990). Scrapie prion proteins accumulate in the cytoplasm of persistently infected cultured cells. *J Cell Biol* **110**, 2117-2132.

Uryu, M., Karino, A., Kamihara, Y. & Horiuchi, M. (2007). Characterization of prion susceptibility in Neuro2a mouse neuroblastoma cell subclones. *Microbiol Immunol* **51**, 661-669.

Ushiki-Kaku, Y., Endo, R., Iwamaru, Y., Shimizu, Y., Imamura, M., Masujin, K., Yamamoto, T., Hattori, S., Itohara, S., Irie, S. & Yokoyama, T. (2010). Tracing conformational transition of abnormal prion proteins during interspecies transmission by using novel antibodies. *J Biol Chem* **285**, 11931-11936.

Veith, N. M., Plattner, H., Stuermer, C. A., Schulz-Schaeffer, W. J. & Burkle, A. (2009). Immunolocalisation of PrPSc in scrapie-infected N2a mouse neuroblastoma cells by light and electron microscopy. *Eur J Cell Biol* **88**, 45-63.

Vey, M., Pilkuhn, S., Wille, H., Nixon, R., DeArmond, S. J., Smart, E. J., Anderson, R. G., Taraboulos, A. & Prusiner, S. B. (1996). Subcellular colocalization of the cellular and scrapie prion proteins in caveolae-like membranous domains. *Proc Natl Acad Sci U S A* **93**, 14945-14949.

Wolf, H., Hossinger, A., Fehlinger, A., Buttner, S., Sim, V., McKenzie, D. & Vorberg, I. M. (2015). Deposition pattern and subcellular distribution of disease-associated prion protein in cerebellar organotypic slice cultures infected with scrapie. *Front Neurosci* **9**, 410.

Yamasaki, T., Baron, G. S., Suzuki, A., Hasebe, R. & Horiuchi, M. (2014a). Characterization of intracellular dynamics of inoculated PrP-res and newly generated PrP(Sc) during early stage prion infection in Neuro2a cells. *Virology* **450-451**, 324-335.

Yamasaki, T., Suzuki, A., Hasebe, R. & Horiuchi, M. (2014b). Comparison of the

anti-prion mechanism of four different anti-prion compounds, anti-PrP monoclonal antibody 44B1, pentosan polysulfate, chlorpromazine, and U18666A, in prion-infected mouse neuroblastoma cells. *PLoS One* **9**, e106516.

Yamasaki, T., Suzuki, A., Shimizu, T., Watarai, M., Hasebe, R. & Horiuchi, M. (2012). Characterization of intracellular localization of PrP(Sc) in prion-infected cells using a mAb that recognizes the region consisting of aa 119-127 of mouse PrP. *J Gen Virol* **93**, 668-680.

653 ***Figure legends***

654

655 ***Figure 1. PrP^{Sc}-specific staining in immortalized cell lines persistently infected with 22L***
656 ***prion strain.*** (a) Detection of PrP^{Sc} in ScN2a-3-22L with [Gdn(+)] or without
657 GdnSCN-pretreatment [Gdn(−)]. Alexa Fluor 647-conjugated mAb 132 (red) and Alexa Fluor
658 488-conjugated mAb 8D5 (green) were used for direct detection of PrP^{Sc}. Nuclei were
659 counterstained with 4',6-Diamidino-2-phenylindole (DAPI) (blue). (b and c) Double staining
660 of PrP^{Sc} using mAbs 132 and 8D5. PrP^{Sc} in GdnSCN pretreated ScN2a-3-22L cells (b) and
661 ScGT1-7-22L cells (c) was simultaneously detected by Alexa Fluor-labeled mAbs 132 (red)
662 and 8D5 (green). Magnified images of the boxed areas in the leftmost panels are shown in the
663 three panels on the right. Arrowheads show representative granular stains with mAb 8D5 near
664 the edges of cells. Arrows indicate representative overlapping stains with mAbs 132 and 8D5.
665 Scale bars: (a and c) 10 μm, (b) 5 μm.

666

667 ***Figure 2. Purity of primary neuronal culture from mouse cerebra.*** (a) The scheme for the
668 Ara-C treatment. Cells were treated with 0.25 and 0.125 μM of Ara-C from 4 to 6 and 7 to 10
669 div, respectively, and Ara-C was completely removed at 11 div, corresponding to 4 dpi. (b)
670 Visualization of neurons and activated astrocytes in primary neuronal cultures. Mock-infected
671 cultures at 7, 14, and 28 div were stained with MAP2 (gray), GFAP (red), and DAPI (blue).
672 Scale bars: 50 μm. (c) Kinetics of the expression of GFAP and β-III tubulin.

673

674 ***Figure 3. Generation of PrP^{Sc} in CNs.*** (a) Kinetics of PrP-res generation in CNs. PK-treated
675 cell lysates were subjected to SDS-PAGE and following immunoblot using anti-PrP antibody

mAb 31C6. Purified recombinant PrP (rPrP) (5 ng lane^{-1}) was used as a standard for the quantification. The sample at 0 dpi was harvested before the exposure to prions. Figures show representative immunoblot images of PrP-res. The graph on the right shows quantitative results (means and standard deviations of triplicate experiments, except 22L or Chandler strain-infected CNs at 35 dpi, which are shown as a single datum). Values indicate the total amount of PrP-res in each well. (b) PrP^{Sc} in CNs. PrP^{Sc} in prion-infected CNs was detected by PrP^{Sc}-specific immunostaining using mAb 132 (green) at 7, 14, and 28 dpi. Arrows indicate string-like PrP^{Sc} stains. Neuronal cell bodies and dendrites were identified by the staining of MAP2 (gray), and nuclei were counterstained with DAPI (blue). Scale bars: 10 μm.

Figure 4. PrP^{Sc}-specific double staining of prion-infected CNs. CNs infected with 22L, Chandler, or Obihiro prion strain were fixed and pretreated with GdnSCN and stained simultaneously with Alexa Fluor 647-conjugated mAb 132 (red) and Alexa Fluor 488-conjugated mAb 8D5 (green) at 14 dpi. Neurons were visualized with anti-MAP2 antibody (gray), and nuclei were stained with DAPI (blue). Boxed areas in merged images are enlarged in the corresponding rightmost columns. Closed arrows indicate string-like stains of PrP^{Sc} by mAbs 132 and 8D5, and open arrows indicate granular stains of PrP^{Sc}. Arrowheads show representative overlapping stains with mAbs 132 and 8D5. Scale bars: 10 μm.

Figure 5. Detection of PrP^{Sc} on the cell surface of living CNs by mAb 8D5. CNs at 14 dpi were incubated with Alexa Fluor 488-conjugated mAb 8D5 at 37 °C for 1 h without fixation, permeabilization, or denaturation. Upper panels show the signals detected by mAb 8D5

(green), and lower panels show the merged images with a differential interference contrast image (DIC). Scale bars: 20 μm

Figure 6. Colocalization analysis of PrP^{Sc} in cells. (a) A scheme for the colocalization analysis. First, 3D-fluorescent images were constructed from Z-stack images, and fluorescence-positive 3D-regions, "surface", were created by IMARIS software. Next, PrP^{Sc}-positive surfaces were broken down into voxel(s), the minimum unit of 3D-images, for following quantification. Voxel(s) positive for mAb 132, mAb 8D5, or both mAbs were counted, and the proportion to the total voxels positive for PrP^{Sc} detected in cells was calculated by dividing the voxel number of each population by that of total PrP^{Sc}. (b) Proportions of PrP^{Sc} populations with different immunoreactivity. Each bar shows the percentage of PrP^{Sc} detected by only mAb 132 (red) or 8D5 (green), or both mAbs (yellow) in cells. The numbers in yellow bar indicate the percentage of PrP^{Sc} positive for both mAbs. Cell types used for this analysis are shown at the bottom: ScN2a-22L and ScGT1-7-22L cells as immortalized cell lines; CNs infected with 22L (CN-22L), Chandler (CN-Ch), or Obihiro (CN-Obi) strain (at 14 dpi). (c) Proportions of PrP^{Sc} detected by mAb 132 or mAb 8D5 in three cell types. The proportions of mAb 132-positive or mAb 8D5-positive PrP^{Sc} to total PrP^{Sc} in the corresponding cells were picked out from (b). Graphs represent the means and standard deviations of 9 wells from 3 independent experiments for N2a-3 and GT1-7 cells, and those of 6 wells from 2 independent experiments for CNs. Z-stack images were acquired from three to four view fields per well, which contained 10 cells for N2a-3, 7 cells for GT1-7, or 4 cells for CNs. Statistical analysis was done by one-way ANOVA, and *post hoc*

720 comparisons were carried out using Tukey-Kramer multiple comparisons test. *, $p<0.05$; **
721 $p<0.01$.
722
723 ***Figure 7. Biochemical properties of PrP molecules in cells.***
724 (a) Total PrP molecules in cells. PK-untreated cell lysates from N2a-3, GT1-7 and primary
725 cerebral neurons (CNs, at 21 dpi) were subjected to immunoblotting using mAbs 110 and
726 31C6. Lysate equivalent to 3 μg total protein was loaded onto each lane. Arrows indicate full
727 length PrP. Un, uninfected; Inf, infected with 22L prion strain; rPrP, recombinant PrP as a
728 marker. (b) Immunoprecipitation of PrP^{Sc} with mAb 8D5. Immunoprecipitates from GT1-7
729 (GT1) or ScGT-17-22L (ScGT1) cells with mAb 8D5 or negative control mAb (NC) were
730 subjected to immunoblotting using mAb 110 that recognizes the epitope in the octapeptide
731 repeat at aa 59–65 and 83–89.
732

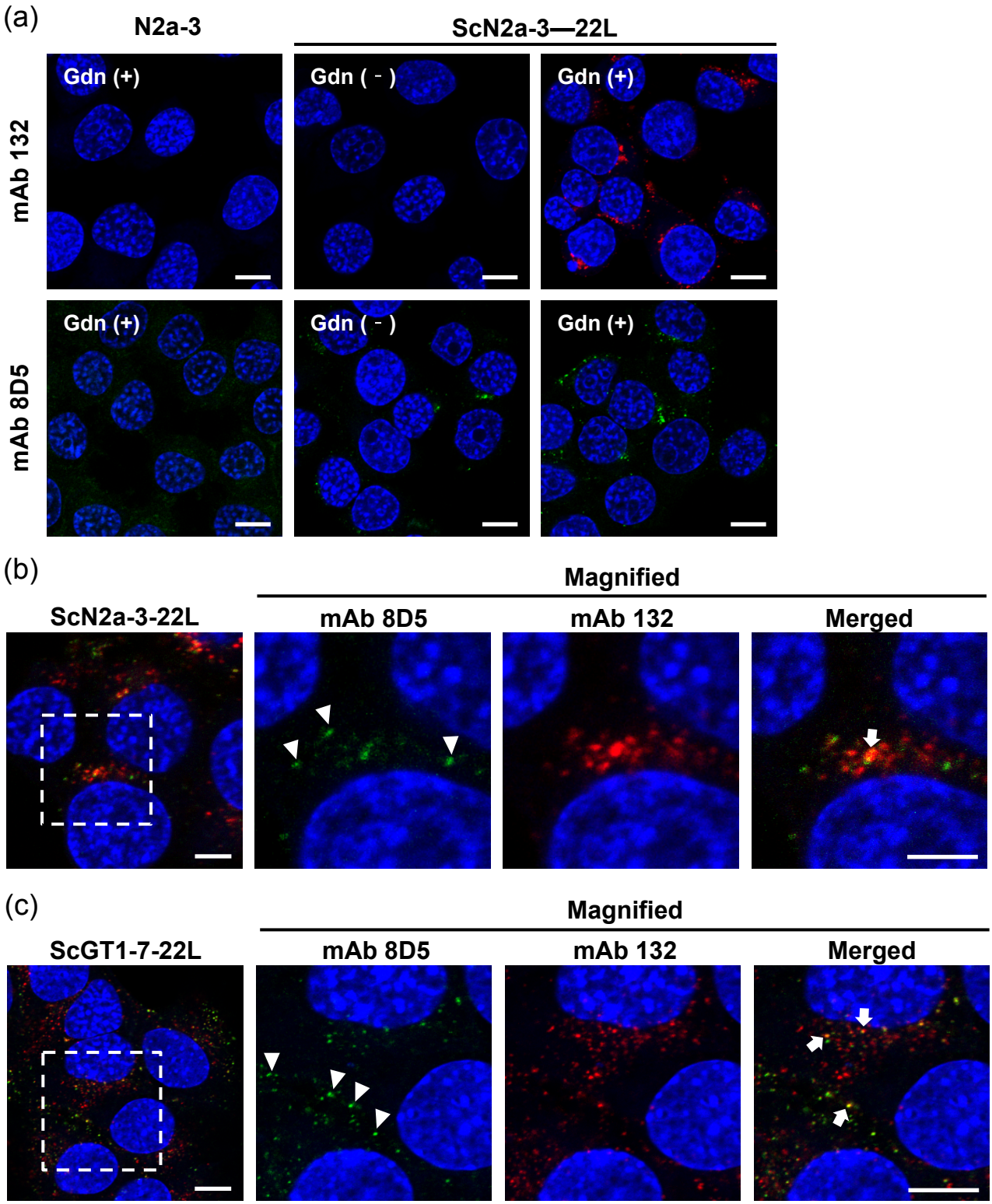

Fig.1 Tanaka et al.

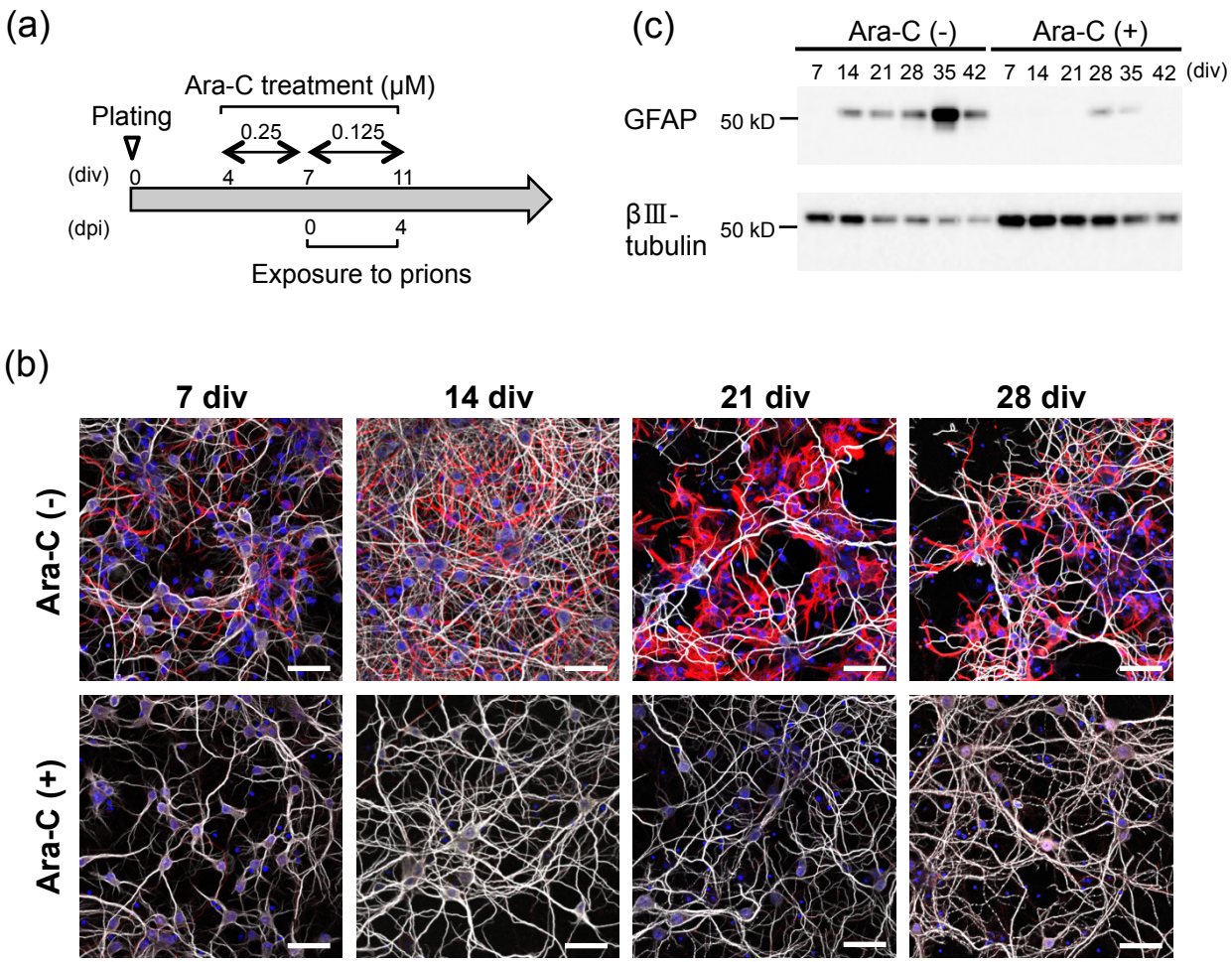

Fig.2 Tanaka et al.

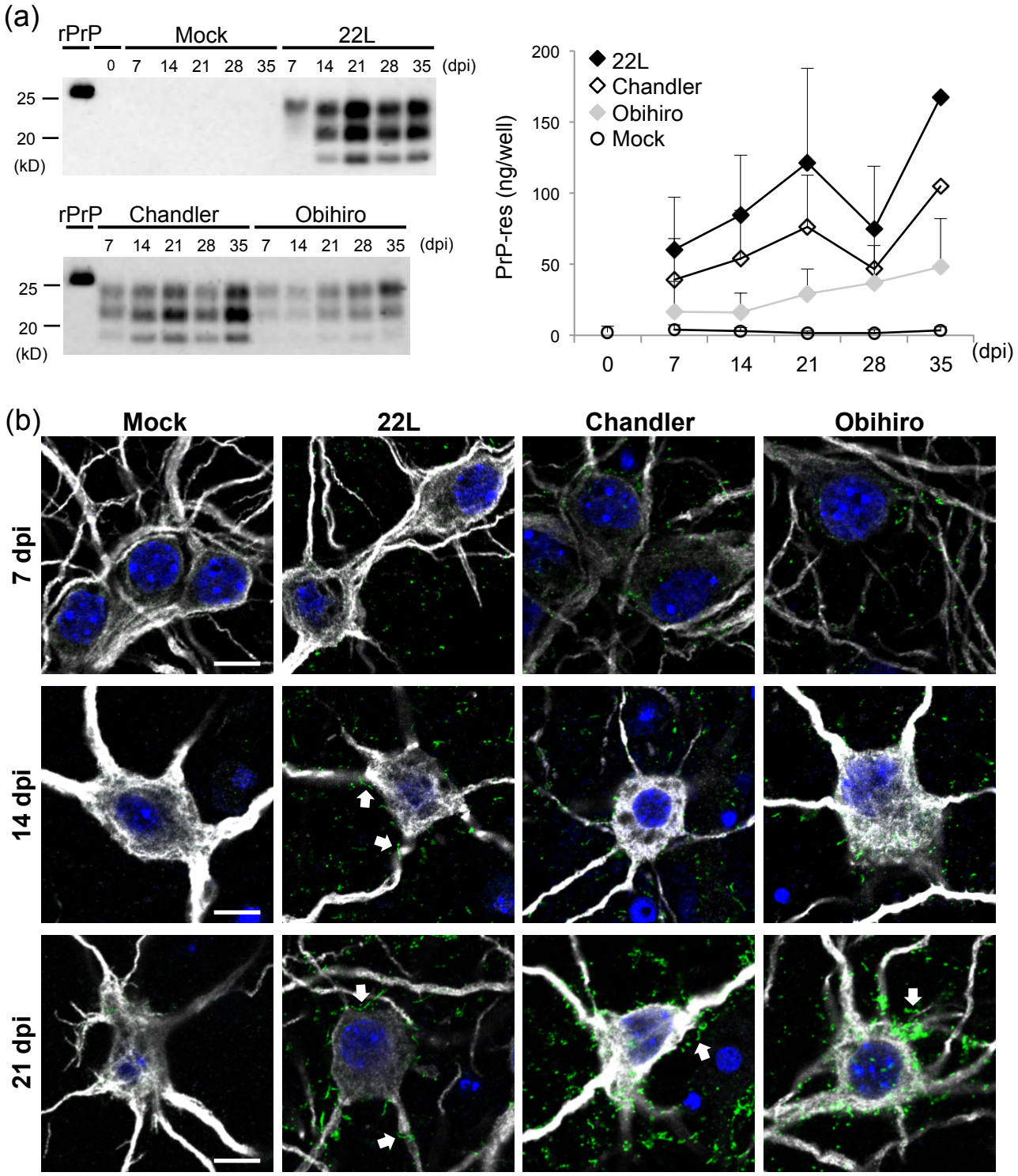

Fig.3 Tanaka et al.

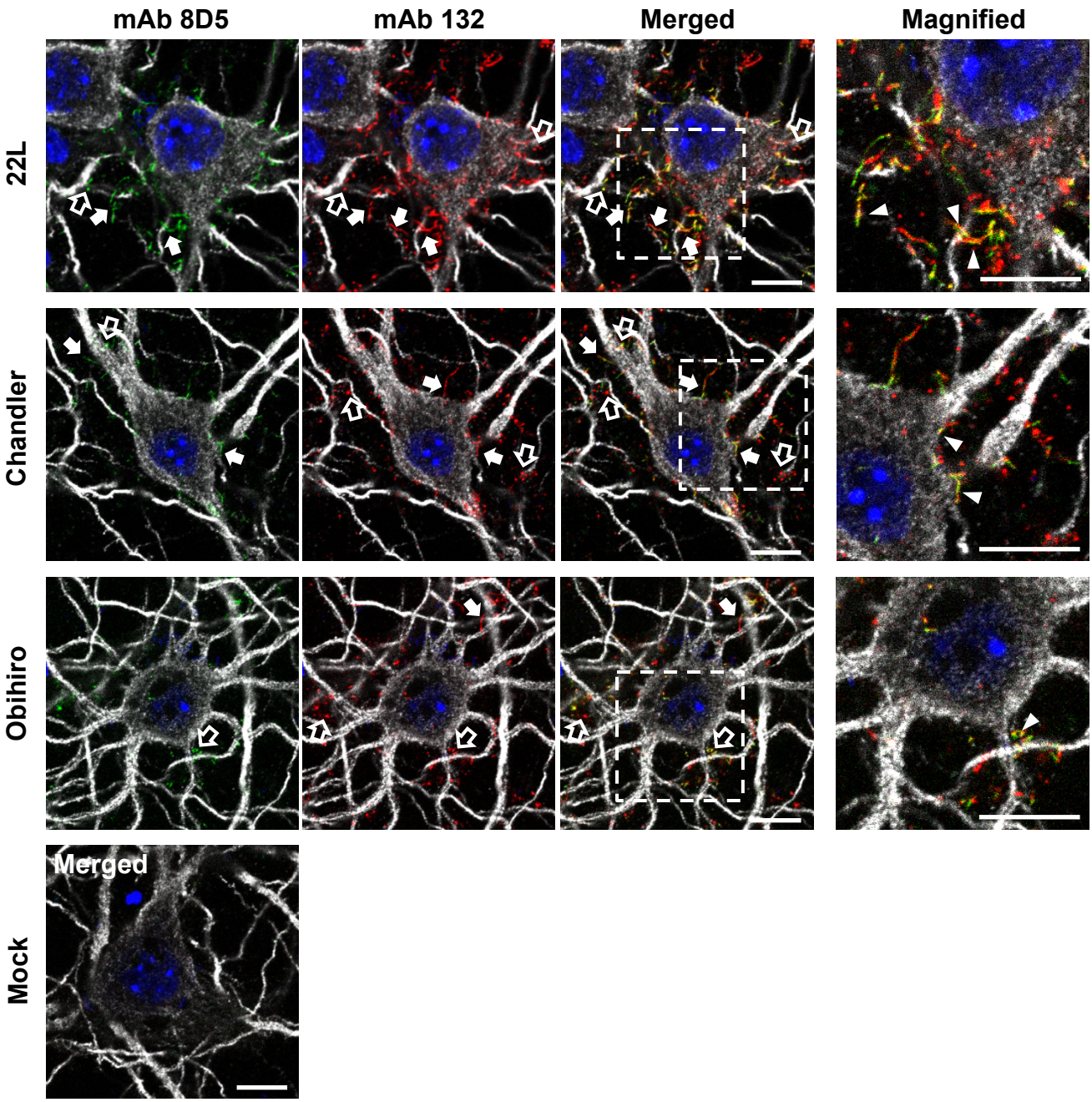

Fig.4 Tanaka et al.

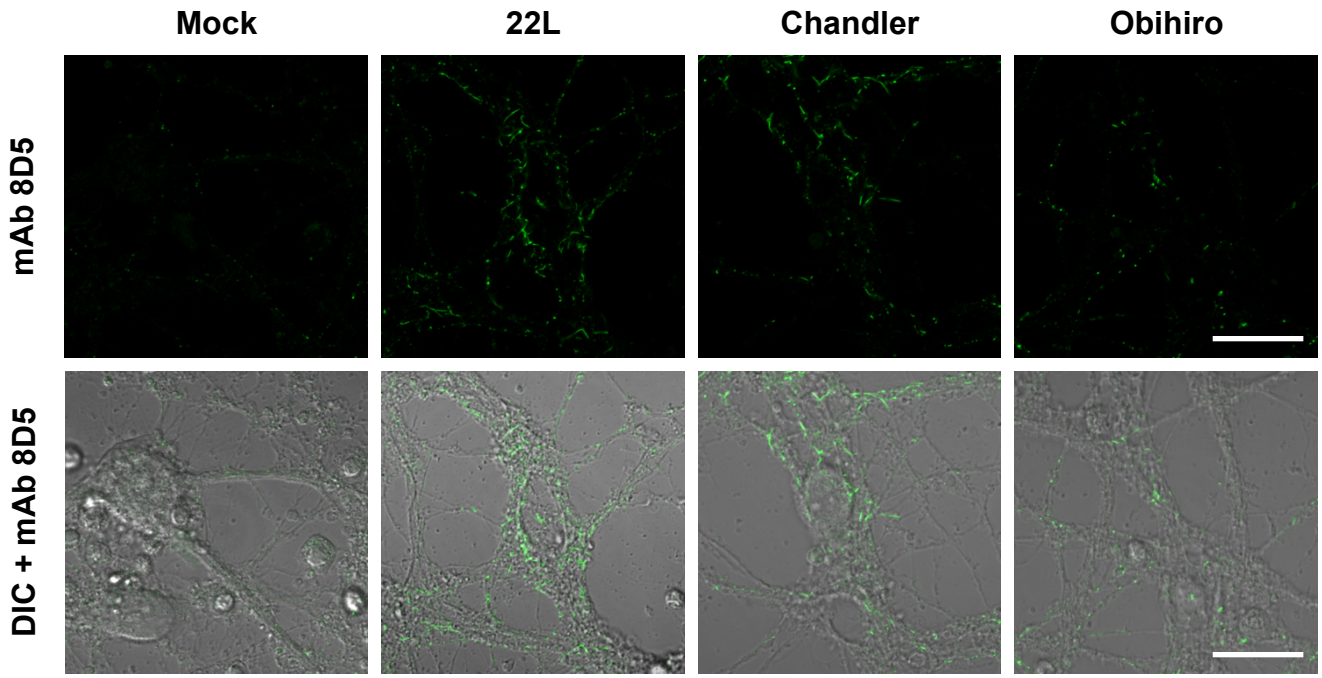

Fig.5 Tanaka et al.

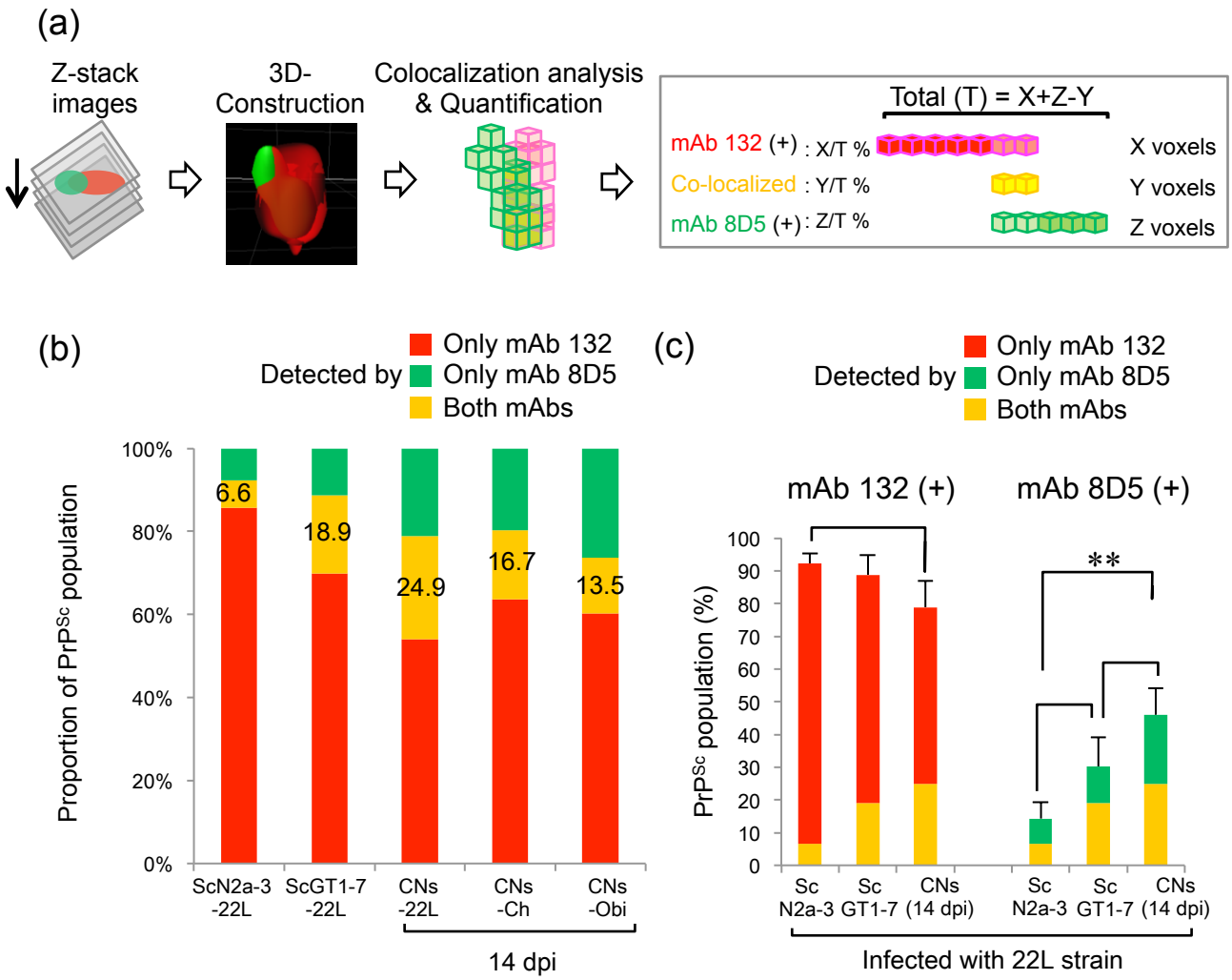

Fig.6 Tanaka et al.

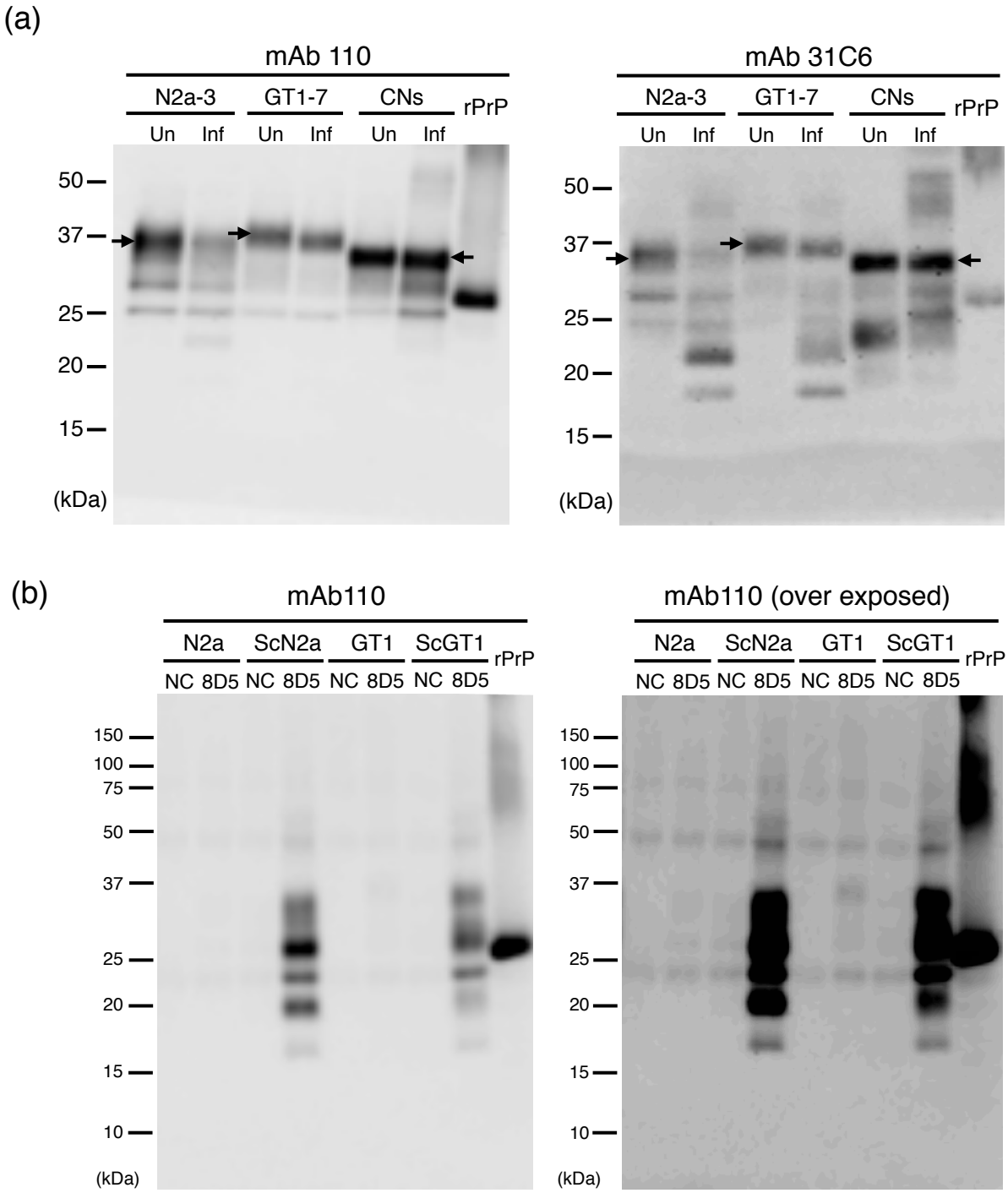

Fig.7 Tanaka et al.